Spin dynamics of the spin-Peierls transition in a quantum Heisenberg antiferromagnetic chain

Atsuko Kouzuki and Kazuko Kawasaki
Department of Physics, Nara Women's University, Nara 630-8506, Japan

Katsuhiro Nakamura
Department of Applied Physics, Osaka City University, Osaka 558-8585, Japan
(Received 29 April 1999; revised manuscript received 29 July 1999)

We investigate full dynamical behaviors of the spin-Peierls transition in $S=1/2$ Heisenberg antiferromagnetic chains by means of two-time Green's functions. The effect of temperature-dependent lattice displacements is incorporated self-consistently. Depending on temperature T and transfer wave number k, the imaginary part of the dynamical susceptibility $\chi''_{zz}(k,\omega)$ shows rich structures: At $T=0$, it is nonvanishing in the frequency region $\Omega_M(k)<\Omega$ $(\equiv\hbar\omega/J)<\Omega_H(k)$. $\Omega_M(k)$ denotes a lower edge of a triplet magnetic excitation continuum, and is finite at $k=0$ due to lattice distortion. The upper edge $\Omega_H(k)$ increases as $k=0$ is approached, which is completely different from the feature without lattice distortion. An asymmetric line shape of $\chi''_{zz}(k,\omega)$ is found with a peak at the frequency slightly higher than $\Omega_M(k)$. At $0<T<T_{SP}$ (spin-Peierls transition point) there appears another structure due to thermal fluctuations in the lower-frequency region, $0<\Omega<\Omega_L(k)$. Since $\Omega_L(k)<\Omega_M(k)$, the forbidden band always exists at $T<T_{SP}$. Above T_{SP}, $\chi''_{zz}(k,\omega)$ reduces to a smooth curve characterized by a single broad maximum. These features in dynamics are systematically explained in terms of different quasiparticle scattering processes proper to the spin-Peierls phase. The results are compared with recent experimental data of neutron scattering for the inorganic compound $CuGeO_3$. [S0163-1829(99)06441-3]

I. INTRODUCTION

The spin-Peierls (s-P) transition is known as a magnetic analogue of the Peierls instability in electron-phonon systems;[1,2] coupling of the $S=1/2$ spin chain to three-dimensional phonons of the crystal lattice induces spontaneously a lattice distortion such that the nearest-neighboring magnetic ions move alternately closer and further apart. This leads to a formation of a lattice of singlet pairs, where the first excited state is separated from the ground state by an energy gap. Major theoretical investigations on the spin-Peierls transition were carried out for the quasi-one-dimensional (1D) organic compounds TTF-CuBDT and TTF-AuBDT, etc.,[3] more than two decades ago. At that time, theoretical studies concentrated on the thermodynamic properties, for instance, temperature dependence of the lattice distortion, specific heat, and anomalous behavior of the uniform susceptibility. These results are described in an excellent review article.[4] Except for exact numerical analyses of ''finite'' spin chains, however, only a few theoretical efforts have been devoted to the systematic analysis of dynamical susceptibilities of the system with temperature-dependent lattice distortions. While the dynamic correlation functions at the limiting temperatures $T=0$ and ∞ were calculated for the 1D antiferromagnet of $S=1/2$ spins with ''T-independent'' alternating exchange interactions,[5] it is essential that, at finite temperatures, lattice spacings should be determined self-consistently to derive the accurate T dependence of dynamic properties.

More recently, experimental reports are growing in number since the characteristic feature of s-P transition was first observed by Hase *et al.* for the inorganic compound $CuGeO_3$,[6] which is suggested to be a quasi-1D spin-Peierls material.[7] The neutron-scattering experiments on this compound provide us various new features of its spin dynamics.[8–13]

In such circumstances, we studied the dynamical behaviors of s-P phase accompanied by T-dependent lattice displacement $\delta(T)$ in the case of 1D XY antiferromagnet[14] that allows a rigorous analysis. To understand the properties of the real s-P magnets like $CuGeO_3$, however, the dynamics should be considered on the basis of the isotropic Heisenberg model.

In this paper, we deal with the 1D Heisenberg model, and investigate theoretically the effect of $\delta(T)$ in the s-P phase on its dynamic properties. We shall not take the bosonization or phase-Hamiltonian approach,[15] whose validity is not well-justified in describing the dynamics covering all wave numbers at all temperatures. The generalized susceptibility $\chi(k,\omega)$ for the s-P phase is calculated by having recourse to the two-time Green's function.[16] In contrast to the XY model, rigorous calculations are not available for the distorted Heisenberg model because of the coupling term $JS_i^zS_j^z$. With the help of the Hartree-Fock approximation for higher-order Green's functions derived from the equations of motion, however, we can evaluate $\chi(k,\omega)$ self-consistently by solving a set of equations for relevant quantities.

The paper is organized as follows: In Sec. II we introduce the model and describe a gap equation. In Sec. III we develop our theory of the generalized longitudinal susceptibility by means of two-time Green's functions.[16] In Sec. IV the numerical calculation of the susceptibility is carried out for arbitrary transfer wave number k, frequency ω, and temperature T. Besides anomalous temperature dependence of the uniform susceptibility, we shall show various features of both static and dynamic susceptibilities that have not so far

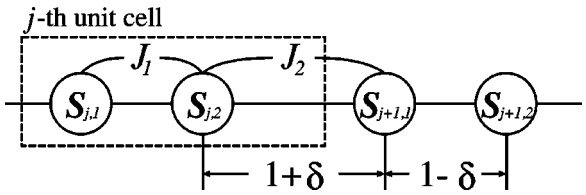

FIG. 1. The jth unit cell containing two spins located at odd $(j,1)$ and even $(j,2)$ sites, respectively. Alternating lattice spacings are $|(j,1)-(j,2)|=1-\epsilon$ and $|(j,2)-(j+1,1)|=1+\epsilon$, taking a lattice constant as unity.

been analyzed theoretically. Rich structures of the imaginary part of the dynamical susceptibility will be explained systematically in terms of different quasiparticle scattering processes proper to the s-P phase. The obtained results are compared with recent experimental data for the compound $CuGeO_3$.[8–13] The paper concludes with summary and discussions in Sec. V.

II. MODEL AND GAP EQUATIONS

Taking the adiabatic approximation that suppresses a kinetic energy of the nuclei, the Hamiltonian for the 1D quantum Heisenberg model of $2N$ spins of $S=1/2$ with lattice displacement is written as

$$\mathcal{H}=\sum_{j=1}^{N}\left[J_1\boldsymbol{S}_{j,1}\cdot\boldsymbol{S}_{j,2}+J_2\boldsymbol{S}_{j,2}\cdot\boldsymbol{S}_{j+1,1}\right]+NC\epsilon^2, \tag{1}$$

where $\boldsymbol{S}_{N+1,1}=\boldsymbol{S}_{1,1}$. The j summation runs over N unit cells with each containing a pair of spins as shown in Fig. 1. The last term on the right-hand side (rhs) of Eq. (1) represents the elastic energy with elastic constant C and lattice distortion ϵ. Alternating exchange interactions $J_1(>0)$ and $J_2(>0)$ are assumed linearly dependent on the static distortion amplitude as

$$J_1=J(1+\delta),\quad J_2=J(1-\delta),$$

where $\delta=\eta\epsilon(\ll 1)$ with $J\eta(>0)$ denoting the spatial derivative of exchange integral. Below, the scaled elastic constant $c\equiv C/\eta^2$ will be employed.

The fermionic representation of the Hamiltonian[17] in Eq. (1) is given by (see Appendix A)

$$\begin{aligned}\mathcal{H}=&\sum_{\lambda}|J(\lambda)|[\alpha_\lambda^\dagger\alpha_\lambda-\gamma_\lambda^\dagger\gamma_\lambda]+(2N)^{-1}\sum_{\lambda_1+\lambda_2=\lambda_3+\lambda_4}\\&\times J(\lambda_4-\lambda_1)\exp[i(\phi_{\lambda_1}-\phi_{\lambda_2}+\phi_{\lambda_3}-\phi_{\lambda_4})/2]\\&\times(\alpha_{\lambda_1}^\dagger-\gamma_{\lambda_1}^\dagger)(\alpha_{\lambda_2}^\dagger+\gamma_{\lambda_2}^\dagger)(\alpha_{\lambda_3}+\gamma_{\lambda_3})(\alpha_{\lambda_4}-\gamma_{\lambda_4})\\&+Nc\delta^2,\end{aligned} \tag{2}$$

where

$$J(\lambda)=\frac{1}{2}(J_1e^{-i\lambda(1-\delta)}+J_2e^{i\lambda(1+\delta)}) \tag{3}$$

and

$$\phi_\lambda=\lambda\delta-\arctan(\delta\tan\lambda). \tag{4}$$

The phase factor $\{\phi_\lambda\}$ has emerged in our moving to new fermions $\alpha_\lambda,\gamma_\lambda$ via the canonical transformation in Eq. (A4).

To deal with the four-fermion terms in Eq. (2), we have recourse to the Hartree-Fock approximation:

$$\alpha_k^\dagger\alpha_k\alpha_{k'}^\dagger\alpha_{k'}\cong-n_k^\alpha n_{k'}^\alpha+n_k^\alpha\alpha_{k'}^\dagger\alpha_{k'}+n_{k'}^\alpha\alpha_k^\dagger\alpha_k,$$

$$\gamma_k^\dagger\gamma_k\gamma_{k'}^\dagger\gamma_{k'}\cong-n_k^\gamma n_{k'}^\gamma+n_k^\gamma\gamma_{k'}^\dagger\gamma_{k'}+n_{k'}^\gamma\gamma_k^\dagger\gamma_k,$$

where $n_\lambda^\alpha=\langle\alpha_\lambda^\dagger\alpha_\lambda\rangle$ and $n_\lambda^\gamma=\langle\gamma_\lambda^\dagger\gamma_\lambda\rangle$. Equation (2) is then rewritten as

$$\begin{aligned}\mathcal{H}_{HF}=&-\frac{1}{2}JN+\sum_\lambda\left[\varepsilon_\lambda^\alpha\alpha_\lambda^\dagger\alpha_\lambda+\varepsilon_\lambda^\gamma\gamma_\lambda^\dagger\gamma_\lambda\right]\\&+N(J_1p_1^2+J_2p_2^2)/4+Nc\delta^2,\end{aligned} \tag{5}$$

where $\varepsilon_\lambda^\alpha$ and $\varepsilon_\lambda^\gamma$ are the quasiparticle spectra,

$$\begin{aligned}\varepsilon_\lambda^\alpha=&|J(\lambda)|+\frac{1}{2}J_1p_1\cos[\lambda(1-\delta)+\phi_\lambda]\\&+\frac{1}{2}J_2p_2\cos[\lambda(1+\delta)-\phi_\lambda]\\=&-\varepsilon_\lambda^\gamma,\end{aligned} \tag{6}$$

with p_1 and p_2 defined as

$$p_1\equiv N^{-1}\sum_\lambda\cos[\lambda(1-\delta)+\phi_\lambda](n_\lambda^\gamma-n_\lambda^\alpha), \tag{7a}$$

$$p_2\equiv N^{-1}\sum_\lambda\cos[\lambda(1+\delta)-\phi_\lambda](n_\lambda^\gamma-n_\lambda^\alpha). \tag{7b}$$

Thus, the free energy of the system is given by

$$\begin{aligned}F=&-JN/2+Nc\delta^2-2\beta^{-1}\sum_\lambda\ln[2\cosh(\beta\varepsilon_\lambda^\alpha/2)]\\&+N(J_1p_1^2+J_2p_2^2)/4,\end{aligned} \tag{8}$$

where $\beta=1/k_BT$. p_1 and p_2 are order parameters arising from the Hartree-Fock treatment of the Heisenberg antiferromagnet exhibiting the alternating coupling. By minimizing the free energy in Eq. (8) with respect to δ, p_1, and p_2, we obtain the gap equations, which determine the temperature dependence of these three parameters:

$$\frac{\partial F}{\partial p_1}=\frac{N}{2}J_1\left[p_1-\frac{1}{N}\sum_\lambda\cos[\lambda(1-\delta)+\phi_\lambda]\tanh\left(\frac{1}{2}\beta\varepsilon_\lambda^\alpha\right)\right]=0, \tag{9a}$$

$$\frac{\partial F}{\partial p_2}=\frac{N}{2}J_2\left[p_2-\frac{1}{N}\sum_\lambda\cos[\lambda(1+\delta)-\phi_\lambda]\tanh\left(\frac{1}{2}\beta\varepsilon_\lambda^\alpha\right)\right]=0, \tag{9b}$$

$$\frac{\partial F}{\partial\delta}=2Nc\delta-\sum_\lambda\tanh\left(\frac{1}{2}\beta\varepsilon_\lambda^\alpha\right)\frac{\partial\varepsilon_\lambda^\alpha}{\partial\delta}+\frac{NJ}{4}(p_1^2-p_2^2)=0. \tag{9c}$$

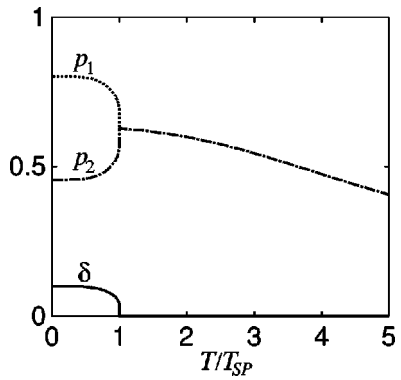

FIG. 2. Temperature dependence of δ, p_1, and p_2 with $c/J=2.35$. This value for the (scaled) elastic constant is used throughout in the following figures.

We note that Eqs. (9a) and (9b) are consistent with definitions of p_1 and p_2 in Eqs. (7a) and (7b), respectively. Using $c/J=2.35$, we shall solve Eqs. (9).

The result of numerical analysis for the gap equations is shown in Fig. 2, which shows the following. (1) $\delta(T)$ becomes nonvanishing below the s-P transition temperature T_{SP} (i.e., in the s-P phase) and grows with decreasing temperature. This behavior of $\delta(T)$ accords with the previous result.[17] (2) $p_1(T)$ and $p_2(T)$, which are degenerate above T_{SP}, show a clear bifurcation below T_{SP}. By using the quantities $p_1(T)$, $p_2(T)$, and $\delta(T)$, the quasiparticle spectra in Eq. (6) are evaluated. While the formalism in Eqs. (2)–(7) is constructed for the s-P phase where the first Brillouin zone is halved, it can also describe the phase above T_{SP} after a slight modification (see the next section). All these results will be used as inputs in the following sections.

III. DYNAMICAL SUSCEPTIBILITY

In order to study the dynamical behavior of the s-P phase, let us first introduce block spin per unit cell (see Fig. 1) as

$$\mathcal{T}^z(l)=S^z_{l,1}+S^z_{l,2}, \tag{10}$$

where $l=1,2,\ldots,N$. Then the retarded Green's function is defined as

$$\langle\langle \mathcal{T}^z(l,t)|\mathcal{T}^z(l',t')\rangle\rangle=-i\theta(t-t')\langle \mathcal{T}^z(l,t)\mathcal{T}^z(l',t') - \mathcal{T}^z(l',t')\mathcal{T}^z(l,t)\rangle, \tag{11}$$

where $\theta(t)$ is the step function and $\langle\rangle$ stands for the thermodynamic average. In Eqs. (10) and (11), indices l and l' run over unit cells.

Experimentally relevant information is available from the frequency- and wave-number-dependent longitudinal complex susceptibility $\chi_{zz}(k,\omega)$. This is related to Fourier transform of the retarded Green's function as follows:

$$\chi_{zz}(k,\omega)=-\frac{g^2\mu^2}{N}\int_{-\infty}^{\infty}d(t-t')\exp[i\omega(t-t')] \times\langle\langle \mathcal{T}^z(-k,t)|\mathcal{T}^z(k,t')\rangle\rangle, \tag{12}$$

where

$$\begin{aligned}\langle\langle \mathcal{T}^z(-k,t)|\mathcal{T}^z(k,t')\rangle\rangle &=\frac{1}{N}\sum_{l,l'}\exp[-ik(l-l')]\langle\langle \mathcal{T}^z(l,t)|\mathcal{T}^z(l',t')\rangle\rangle\\ &=\sum_{\nu}\sum_{\lambda}\{\langle\langle a^\dagger_\lambda(t)a_{\lambda-k}(t)|a^\dagger_\nu(t')a_{\nu+k}(t')\rangle\rangle\\ &\quad+\exp[ik(1-\delta)]\langle\langle b^\dagger_\lambda(t)b_{\lambda-k}(t)|a^\dagger_\nu(t')a_{\nu+k}(t')\rangle\rangle\\ &\quad+\exp[-ik(1-\delta)]\\ &\quad\times\langle\langle a^\dagger_\lambda(t)a_{\lambda-k}(t)|b^\dagger_\nu(t')b_{\nu+k}(t')\rangle\rangle\\ &\quad+\langle\langle b^\dagger_\lambda(t)b_{\lambda-k}(t)|b^\dagger_\nu(t')b_{\nu+k}(t')\rangle\rangle\}.\end{aligned} \tag{13}$$

In deriving the result in Eq. (13), we have exploited the fermion transformations in Eqs. (A1) and their Fourier transformations. The phase factors $\exp[\pm ik(1-\delta)]$ in Eq. (13) are responsible for alternating lattice spacings in the s-P phase.

Using Eqs. (A4) in Eq. (13), the longitudinal dynamical susceptibility reduces to the expression described in terms of four kinds of Green's functions:

$$\begin{aligned}\chi_{zz}(k,\omega)=-\frac{g^2\mu^2}{2N}\sum_{\nu}\sum_{\lambda}\Bigg\{&\left[\cos\frac{\phi_1}{2}+\cos\frac{\phi_2+2k(1-\delta)}{2}\right]\\ &\times\{\langle\langle \alpha^\dagger_\lambda\alpha_{\lambda-k}|\alpha^\dagger_\nu\alpha_{\nu+k}\rangle\rangle_\omega\\ &+\langle\langle \gamma^\dagger_\lambda\gamma_{\lambda-k}|\gamma^\dagger_\nu\gamma_{\nu+k}\rangle\rangle_\omega\}\\ &+\left[\cos\frac{\phi_1}{2}-\cos\frac{\phi_2+2k(1-\delta)}{2}\right]\\ &\times\{\langle\langle \alpha^\dagger_\lambda\gamma_{\lambda-k}|\gamma^\dagger_\nu\alpha_{\nu+k}\rangle\rangle_\omega\\ &+\langle\langle \gamma^\dagger_\lambda\alpha_{\lambda-k}|\alpha^\dagger_\nu\gamma_{\nu+k}\rangle\rangle_\omega\}\Bigg\},\end{aligned} \tag{14}$$

where $\phi_1\equiv\phi_{\nu+k}-\phi_\nu-\phi_\lambda+\phi_{\lambda-k}$ and $\phi_2\equiv\phi_{\nu+k}-\phi_\nu+\phi_\lambda-\phi_{\lambda-k}$. In Eq. (14), the frequency-dependent Green's function

$$\langle\langle A|B\rangle\rangle_\omega\equiv\int_{-\infty}^{\infty}d(t-t')\exp[i\omega(t-t')]\langle\langle A(t)|B(t')\rangle\rangle, \tag{15}$$

satisfies the equation of motion

$$\hbar\omega\langle\langle A|B\rangle\rangle_\omega=\langle[A,B]_-\rangle+\langle\langle[A,\mathcal{H}]_-|B\rangle\rangle_\omega. \tag{16}$$

The second term on the rhs of Eq. (16) is a new Green's function obeying another equation of motion.

In the present system, the equation of motion is, typically,

$$\hbar\omega\sum_{\mu}\langle\langle \alpha^\dagger_\lambda\alpha_{\lambda-k}|\alpha^\dagger_\mu\alpha_{\mu+k}\rangle\rangle_\omega=\sum_{\mu}\langle[\alpha^\dagger_\lambda\alpha_{\lambda-k},\alpha^\dagger_\mu\alpha_{\mu+k}]_-\rangle +\sum_{\mu}\langle\langle[\alpha^\dagger_\lambda\alpha_{\lambda-k},\mathcal{H}]_-|\alpha^\dagger_\mu\alpha_{\mu+k}\rangle\rangle_\omega. \tag{17}$$

The new Green's function on the rhs of Eq. (17) can now be expressed in terms of the original Green's functions through the following decoupling procedure (i.e., in the Hartree-Fock approximation):

$$\begin{aligned}\langle\langle \alpha^\dagger_{k_1}\alpha^\dagger_{k_2}\alpha_{k_3}\alpha_{k_4}|\alpha^\dagger_{\lambda_1}\alpha_{\lambda_2}\rangle\rangle_\omega &\cong n^\alpha_{k_1}\{\langle\langle \alpha^\dagger_{k_2}\alpha_{k_3}|\alpha^\dagger_{\lambda_1}\alpha_{\lambda_2}\rangle\rangle_\omega\delta_{k_1,k_4}\\ &\quad-\langle\langle \alpha^\dagger_{k_2}\alpha_{k_4}|\alpha^\dagger_{\lambda_1}\alpha_{\lambda_2}\rangle\rangle_\omega\delta_{k_1,k_3}\}\\ &\quad+n^\alpha_{k_2}\{\langle\langle \alpha^\dagger_{k_1}\alpha_{k_4}|\alpha^\dagger_{\lambda_1}\alpha_{\lambda_2}\rangle\rangle_\omega\delta_{k_1,k_3}\\ &\quad-\langle\langle \alpha^\dagger_{k_1}\alpha_{k_3}|\alpha^\dagger_{\lambda_1}\alpha_{\lambda_2}\rangle\rangle_\omega\delta_{k_2,k_3}\},\end{aligned}$$

$$\begin{aligned}&\langle\langle \alpha^\dagger_{k_1}\gamma^\dagger_{k_2}\alpha_{k_3}\gamma_{k_4}|\alpha^\dagger_{\lambda_1}\alpha_{\lambda_2}\rangle\rangle_\omega\\ &\quad\cong -n^\gamma_{k_2}\langle\langle \alpha^\dagger_{k_1}\alpha_{k_3}|\alpha^\dagger_{\lambda_1}\alpha_{\lambda_2}\rangle\rangle_\omega\delta_{k_2,k_4},\end{aligned}\tag{18}$$

where $n^{\alpha(\gamma)}_k = 1/(e^{\beta\varepsilon^{\alpha(\gamma)}_k}+1)$.

To facilitate the calculation of the dynamical susceptibility in Eq. (14), we shall deal with a set of the equations of motion for the (decoupled) Green's functions multiplied by the phase factors. To be explicit, let us define the variables $\{X^{uv}_n\}$ and $\{Y^{uv}_n\}$ with $1\leqslant n\leqslant 6$ for each of four combinations of two fermions $u,v=\alpha$ or γ:

$$X^{uv}_n \equiv \frac{1}{N}\sum_\nu f^{uv}_k Q_n(k;\nu),\tag{19a}$$

$$Y^{uv}_n \equiv \frac{1}{N}\sum_\nu h^{uv}_k R_n(k;\nu),\quad n=1,2,\ldots,6,\tag{19b}$$

where $f^{uv}_k(\nu)$ and $h^{uv}_k(\nu)$ are linear combinations of Green's functions:

$$f^{uv}_k(\nu)=\sum_\mu \cos\left[\frac{1}{2}(\phi_{\mu+k}-\phi_\mu)\right]\langle\langle u^\dagger_\nu v_{\nu-k}|v^\dagger_\mu u_{\mu+k}\rangle\rangle_\omega,\tag{20a}$$

$$h^{uv}_k(\nu)=\sum_\mu \sin\left[\frac{1}{2}(\phi_{\mu+k}-\phi_\mu)\right]\langle\langle u^\dagger_\nu v_{\nu-k}|v^\dagger_\mu u_{\mu+k}\rangle\rangle_\omega.\tag{20b}$$

Coefficients $\{Q_n\}$ and $\{R_n\}$ in Eqs. (19) are defined in Appendix B. As shown there, $\{X^{uv}_n\}$ and $\{Y^{uv}_n\}$ prove to satisfy the algebraic equations

$$A^{uv}\boldsymbol{X}^{uv}=\boldsymbol{C}^{uv},\tag{21a}$$

$$A^{uv}\boldsymbol{Y}^{uv}=\boldsymbol{S}^{uv}.\tag{21b}$$

The coefficients $\{A^{uv}\}$, $\{C^{uv}\}$, and $\{S^{uv}\}$ defined in Eqs. (B4) and (B5) are commonly determined by means of the ''core'' Green's function,

$$\mathcal{G}^{uv}_k(\lambda)=\frac{n^u_\lambda - n^v_{\lambda-k}}{\hbar\omega-\varepsilon^v_{\lambda-k}+\varepsilon^u_\lambda}.\tag{22}$$

Therefore $\boldsymbol{X}^{uv}$ and $\boldsymbol{Y}^{uv}$ are also determined by $\mathcal{G}^{uv}_k(\lambda)$ in Eq. (22).

Using the solution for Eqs. (21), the dynamical susceptibility in Eq. (14) is eventually expressed in terms of X^{uv}_n and Y^{uv}_n ($n=1,2$ and $u,v=\alpha$ or γ) as

$$\begin{aligned}\chi_{zz}(k,\omega)=\frac{1}{2}g^2\mu^2[&\Xi^{\alpha\alpha}(k,\omega)+\Xi^{\gamma\gamma}(k,\omega)+\Xi^{\gamma\alpha}(k,\omega)\\ &+\Xi^{\alpha\gamma}(k,\omega)],\end{aligned}\tag{23}$$

with

$$\begin{aligned}\Xi^{uv}(k,\omega)=&-\{1\pm\cos[k(1-\delta)]\}X^{uv}_1+\{1\mp\cos[k(1\\ &-\delta)]\}Y^{uv}_2+\sin[k(1-\delta)](X^{uv}_2-Y^{uv}_1).\end{aligned}\tag{24}$$

The upper and lower signs on the rhs of Eq. (24) are taken for the diagonal ($u=v$) and off-diagonal ($u\neq v$) cases, respectively. In the practical calculation, $N^{-1}\Sigma_\lambda$ is replaced by $\pi^{-1}\int_{-\pi/2}^{\pi/2}d\lambda$.

It should also be noted that for the case of no coupling with lattice displacements, which corresponds to the case $T>T_{SP}$, Eq. (21) reduces to the three component equations derived by Todani and Kawasaki,[18] where the dynamical susceptibility $\chi^{(0)}_{zz}(k,\omega)$ for the uniform (nondimered) phase is given by

$$\chi^{(0)}_{zz}(k,\omega)=-F(k,\omega)/\{J-V(k)F(k,\omega)\},\tag{25a}$$

with

$$\begin{aligned}F(k,\omega)=\Gamma_{0,0}-2&\\ \times\frac{(1+2\Gamma_{2,0})\Gamma^2_{0,1}+(1+2\Gamma_{0,2})\Gamma^2_{1,0}-4\Gamma_{1,0}\Gamma_{0,1}\Gamma_{1,1}}{(1+2\Gamma_{2,0})(1+2\Gamma_{0,2})-4\Gamma^2_{1,1}},&\end{aligned}\tag{25b}$$

$$\Gamma_{m,n}=\frac{J}{N}\sum_\lambda \sin^m\lambda\cos^n\lambda\frac{n_\lambda-n_{\lambda-k}}{\hbar\omega+\varepsilon^{(0)}_\lambda-\varepsilon^{(0)}_{\lambda-k}}.\tag{25c}$$

In Eq. (25c), $\varepsilon^{(0)}_\lambda$, defined in the original first Brillouin zone ($-\pi\leqslant\lambda\leqslant\pi$), is written as

$$\varepsilon^{(0)}_\lambda=J(\cos\lambda-1)+\frac{2J}{N}\sum_\nu[1-\cos(\nu-\lambda)]n_\nu.\tag{25d}$$

Contrary to $\chi^{(0)}_{zz}$ in the uniform case, χ_{zz} in Eq. (24) consists of four kinds of quasiparticle scattering processes.

IV. NUMERICAL RESULTS

A. Static susceptibility ($\omega=0$)

Before analyzing the dynamical properties, we shall briefly describe the wave-number-dependent static susceptibility $\chi_{zz}(k,\omega=0)$ available from Eq. (23). Special interest lies in the uniform mode $k=0$: As shown in Fig. 3, $\chi_{zz}(0,0)$ drops exponentially towards zero at temperatures below T_{SP}, which is consistent with experiments on $CuGeO_3$.[6] This is due to the formation of singlet pairs in the s-P phase that causes both the excitation gap and the complete suppression of the zero-point fluctuation. By contrast, the corresponding susceptibility calculated by Bonner and Fisher[19]

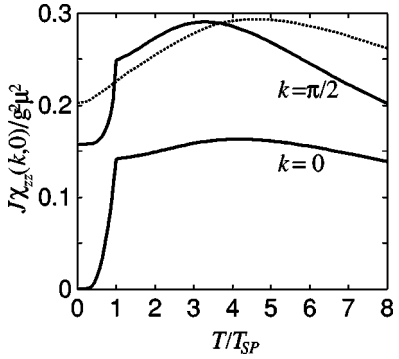

FIG. 3. Static susceptibility $\chi_{zz}(k,0)$ as a function of T for $k=0$ and $\pi/2$. For reference, the temperature dependence of the Bonner-Fisher result (Ref. 19) for ''finite'' chain is indicated by a dotted line.

for a ''finite'' chain without lattice displacement remains constant at $T=0$ as indicated by a dotted line in Fig. 3, because of the gapless low-lying excitation (i.e., Goldstone mode). The static susceptibility is illustrated also for a nonuniform mode, for instance, $k=\pi/2$ in Fig. 3. At $T\leqslant T_{SP}$, $\chi_{zz}(k,0)$ shows a drastic decay in the temperature dependence as in the case of $k=0$, but its values are finite at $T=0$.

$\chi_{zz}(k,0)$ is shown as a function of k in Fig. 4 for three cases of $T/T_{SP}=0$, 0.71, and 1.42. It is interesting to note that, at $T/T_{SP}<1$, $\chi_{zz}(k,0)$ displays a single broad maximum at $k=\pi/2$, i.e., the zone boundary (ZB) of the s-P phase due to doubling of the unit cell, whereas, at $T/T_{SP}>1$, its maximum moves to π, i.e., ZB of the uniform phase.

B. Dynamical susceptibility ($\omega\neq 0$)

The dynamical susceptibility in Eq. (23) is written as

$$\chi(k,\omega)=\chi'(k,\omega)-i\chi''(k,\omega), \tag{26}$$

where $\chi'(k,\omega)$ and $\chi''(k,\omega)$ mean the real and imaginary part of $\chi(k,\omega)$, respectively. Experimental information concerning the dynamical properties of the system is analyzed by investigation of $\chi''(k,\omega)$,[20] which is related directly to the neutron-scattering spectrum as

$$S(k,\omega)=A(k)\frac{e^{\hbar\omega\beta}}{e^{\hbar\omega\beta}-1}\chi''_{zz}(k,\omega). \tag{27}$$

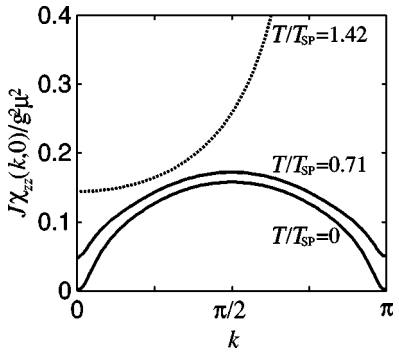

FIG. 4. Static susceptibility $\chi_{zz}(k,0)$ versus wave number k at temperatures $T/T_{SP}=0$ and 0.71 (solid lines) and $T/T_{SP}=1.42$ (dotted line).

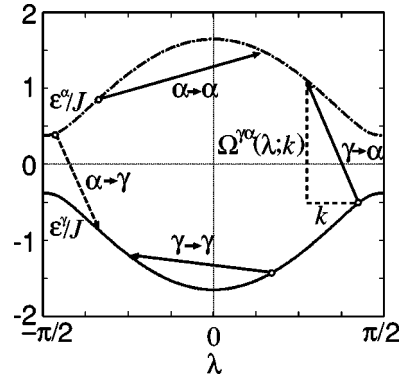

FIG. 5. Schematic illustration of four kinds of quasiparticle scattering processes. For instance, scattering process $\gamma\to\alpha$ implies a particle-hole creation with absorption energy $\hbar\omega^{\alpha\gamma}(\lambda;k)$ and transfer wave number k, while opposite process $\alpha\to\gamma$ means energy emission.

In the above equation, $A(k)$ denotes a form factor characterized by the transfer wave number $k=|k_0-k_1|$, and absorption (or emission) energy is given by $\hbar\omega=E_0-E_1=(k_0^2-k_1^2)/(2m)$, where the initial and final states of the neutron have the wave numbers k_0 and k_1, respectively.

The function $\chi''_{zz}(k,\omega)$ in Eq. (23) consists of four kinds of terms, each corresponding to its proper quasiparticle scattering process as illustrated in Fig. 5. This interpretation is acceptable because each term Ξ^{uv} in Eq. (23) is described by the Green's function $\mathcal{G}_k^{uv}(\lambda)$ in Eq. (22) whose imaginary part is proportional to $\delta(\hbar\omega-\varepsilon^v_{\lambda-k}+\varepsilon^u_{\lambda})$. The first two terms with superscripts $\alpha\alpha$ and $\gamma\gamma$ on the rhs of Eq. (23)

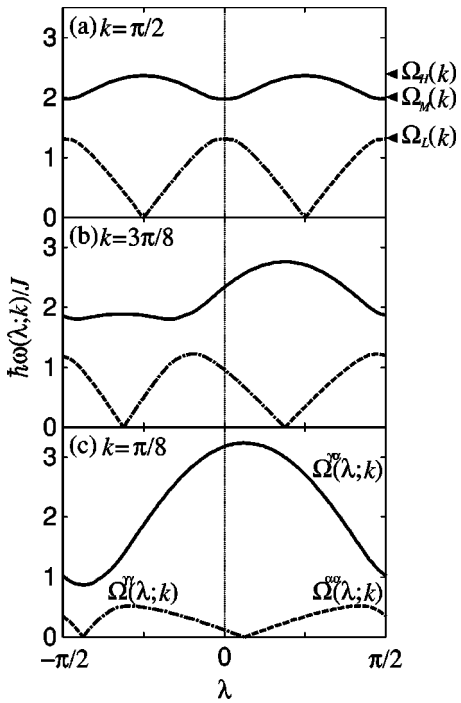

FIG. 6. Reduced transfer energy $\Omega(\lambda;k)$ versus wave number λ at $T/T_{SP}=0.007$ for several transfer wave numbers: (a) $k=\pi/2$; (b) $k=3\pi/8$; (c) $k=\pi/8$. These features are almost identical to those at $T=0$ because lattice distortion is almost saturated at $T/T_{SP}\leqslant 0.5$ (see Fig. 2).

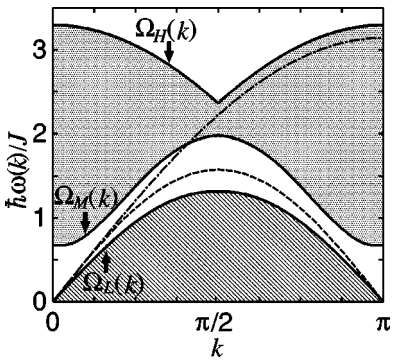

FIG. 7. Dispersion curves for $\Omega_L(k)$, $\Omega_M(k)$, and $\Omega_H(k)$ at $T/T_{SP}=0.007$. Lower- and upper-frequency absorptions are allowed in the region denoted by hatched and dotted areas, respectively. For reference, the des Cloizeaux–Pearson spin-wave dispersion ($\pi/2J|\sin k|$) and the upper edge of the magnetic continuum [$\pi J|\sin(k/2)|$] without coupling to lattice displacement are demonstrated by dashed and dotted-dashed lines, respectively.

imply the quasiparticle scattering within each of the upper α and lower γ bands, respectively, and the third term describes the scattering from γ to α band or the creation of a pair of particles (in α band) and hole (in γ band). The last term represents the reversed scattering from α to γ band, giving no contribution to $\chi''_{zz}(k,\omega)$, since the energy conservation is not satisfied in the absorption process ($\omega \geqslant 0$).

To evaluate $\chi''_{zz}(k,\omega)$, coefficients A, C, S, and Γ in Eqs. (B4) and (B5) should be obtained. With use of the identity $1/(x+i\varepsilon)=\mathcal{P}(1/x)-i\pi\delta(x)$, the integrations of $\mathcal{G}^{uv}_k(\lambda)$ in Eqs. (B4) and (B5) are facilitated by resorting to the formula

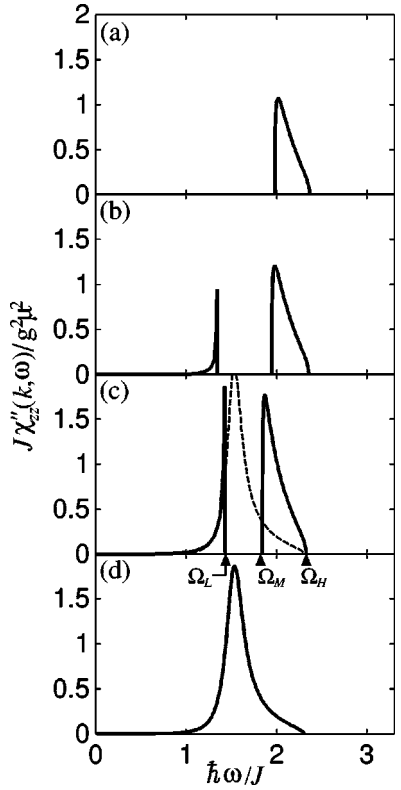

FIG. 8. Imaginary part of dynamical susceptibility $\chi''_{zz}(k,\omega)$ for $k=\pi/2$: (a) $T/T_{SP}=0$; (b) $T/T_{SP}=0.71$; (c) $T/T_{SP}=0.95$; (d) $T/T_{SP}=1.07$. For reference, $\chi''^{(0)}_{zz}(k,\omega)$ without lattice coupling is also illustrated by a dotted line in case (c).

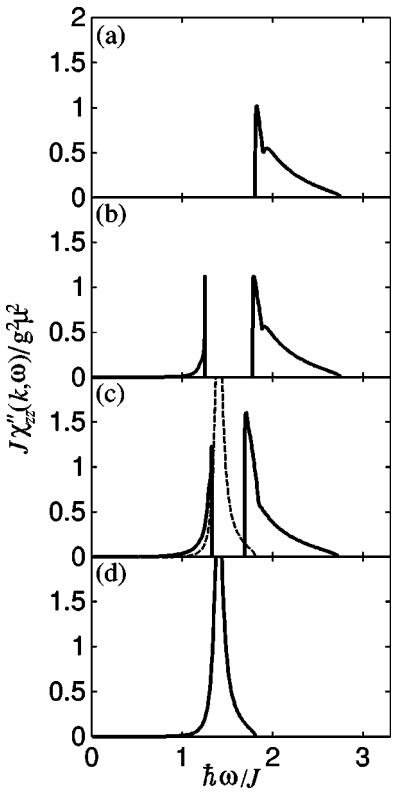

FIG. 9. The same as in Fig. 8 but for $k=3\pi/8$.

$$\delta[\hbar\omega-\hbar\omega(\lambda;k)]=\sum_j \left|\frac{d\hbar\omega(\lambda;k)}{d\lambda}\right|^{-1}_{\lambda=\lambda_j}\delta(\lambda-\lambda_j), \qquad (28)$$

where $\{\lambda_j\}$ are determined by

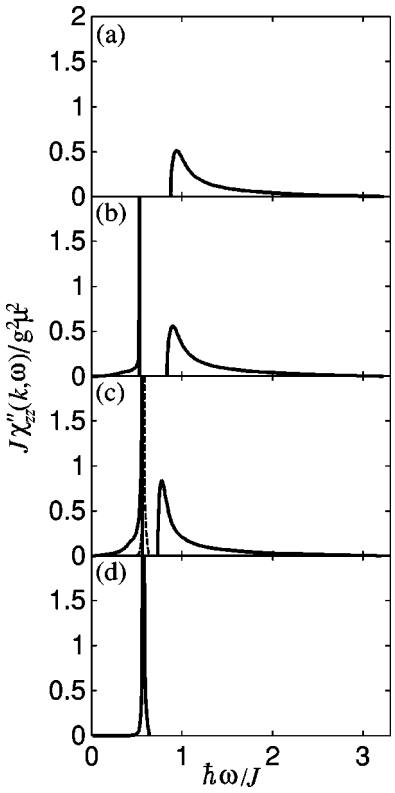

FIG. 10. The same as in Fig. 8 but for $k=\pi/8$.

$$\omega-\omega(\lambda;k)=0. \tag{29}$$

In the case of $u\rightarrow v$ scattering, for example,

$$\hbar\omega(\lambda;k)=\hbar\omega^{uv}(\lambda;k)=\varepsilon^{v}_{\lambda-k}-\varepsilon^{u}_{\lambda}. \tag{30}$$

Obviously, $\chi''_{zz}(k,\omega)$ is nonvanishing in the ω region, where density of states $d\lambda/d\omega(\lambda;k)$ survives.

In Fig. 6 the reduced absorption energy $\Omega^{uv}(\lambda;k)(\equiv\hbar\omega^{uv}/J)$ with $k=\pi/2$, $3\pi/8$, and $\pi/8$ are depicted against wave number λ for all three kinds of absorption processes at $T/T_{SP}=0.007$. We shall define the maximum and minimum of the upper branch $\Omega^{\gamma\alpha}(\lambda;k)$ as $\Omega_H(k)$ and $\Omega_M(k)$, respectively. Similarly $\Omega_L(k)$ is defined as the maximum of the lower branch $\Omega^{uu}(\lambda;k)$ (for $u=\alpha$ or γ). Their wave-number-dependent curves are plotted in Fig. 7 at $T/T_{SP}=0.007$.

Structures of the function $\chi''_{zz}(k,\omega)$ are shown in Figs. 8–10, for several fixed temperatures and wave numbers k. First, let us focus on the limiting case $T\rightarrow 0$ [see Figs. 8(a), 9(a), and 10(a)]. In the case of $k=\pi/2$ in Fig. 8(a), $\chi''_{zz}(k,\omega)$ is composed of a single peak at the frequency slightly higher than $\Omega_M(k)$, and its spectrum is bounded by $\Omega_M(k)\leqslant\Omega\leqslant\Omega_H(k)$. This is explained as follows: In the limit $T\rightarrow 0$, $\tanh(\beta\varepsilon/2)$ reduces to the step function $\theta(\varepsilon)$ because $n^{\alpha}(\lambda)\rightarrow 0$ and $n^{\gamma}(\lambda)\rightarrow 1$. So, only the third term on the rhs of Eq. (23) arising from the particle-hole creation contributes to $\chi''_{zz}(k,\omega)$. In other words, the triplet ($S=1$) magnon excitation formed via interband ($\gamma\rightarrow\alpha$) transition constitutes a continuum with the lower and upper edges, $\Omega_M(k)$ and $\Omega_H(k)$, respectively. The same argument applies to cases of $k=3\pi/8$ and $\pi/8$ in Figs. 9(a) and 10(a), respectively. As k departs from $\pi/2$, however, $\Omega_M(k)$ is decreased and $\Omega_H(k)$ is increased (see also Fig. 7). k dependence of $\Omega_M(k)$ constitutes the spin-wave dispersion $\omega^{SW}(k)$ $[\equiv J\Omega_M(k)/\hbar]$, and exhibits a finite gap at $k=0$. This should be compared with the gapless des Cloizeaux–Pearson spin-wave dispersion[21] $\hbar\omega(k)=(\pi/2)J|\sin k|$. Moreover, the increase of $\Omega_H(k)$ as $k\rightarrow 0$ is in marked contrast with the behavior of the upper edge of the magnetic continuum $[\pi J|\sin(k/2)|]$ in the case of no coupling with lattice displacement.[21]

As shown in Figs. 5 and 6, the nonvanishing width of the triplet magnon continuum $\Delta\Omega(k)[=\Omega_H(k)-\Omega_M(k)]$ is given by

$$\Delta\Omega(k)=\begin{cases} 2(\varepsilon^{\alpha}_{0}-\varepsilon^{\alpha}_{\pi/2})=2J(1-\delta)(1+p_2) & \text{at the zone center } k=0 \\ 2\varepsilon^{\alpha}_{\pi/4}-\varepsilon^{\alpha}_{\pi/2}-\varepsilon^{\alpha}_{0}=J\left[\sqrt{2}-(1+\delta)(1+p_1)+\dfrac{1}{\sqrt{2}}\{p_1(1+2\delta)+p_2(1-2\delta)\}\right] & \text{at the zone boundary } k=\pi/2. \end{cases} \tag{31}$$

Thus $\Delta\Omega(0)>\Delta\Omega(\pi/2)$. If the system is free from the lattice distortion, the opposite relation $\Delta\Omega^{0}(0)<\Delta\Omega^{0}(\pi/2)$ is obtained: In fact, the present approach yields $\Delta\Omega^{0}(0)=0$ and $\Delta\Omega^{0}(\pi/2)=2(1+2/\pi)(|\sin(\pi/4)|-(1/2)|\sin(\pi/2)|)$ $\simeq 2.98$. [Note the exact value,[22] i.e., $\Delta\Omega^{0}(\pi/2)\simeq 2.85$.] The completely different k dependence of $\Delta\Omega(k)$ between the cases with and without coupling to the lattice dispacement is due to the bifurcation of the quasienergy spectra in the dimerized case (see Fig. 7).

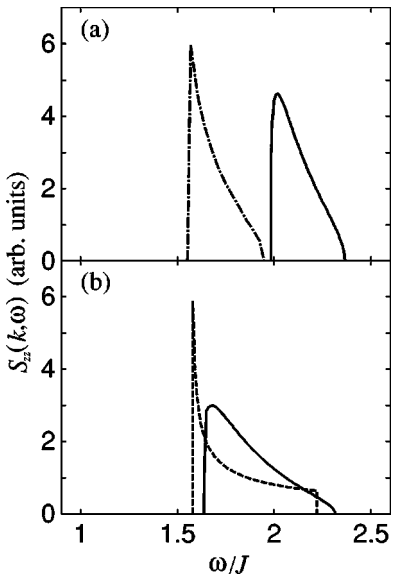

FIG. 11. Comparison of $S_{zz}(k=\pi/2,\omega)$ at $T=0$ between the present (solid line) and previous theoretical [dotted-dashed line for US (Ref. 23) and dashed line for MBB (Ref. 22)] results: (a) case with coupling to lattice displacement; (b) case without coupling to lattice displacement.

The Fourier transform of the dynamical correlation function $S_{zz}(k=\pi/2,\omega)$ at zero temperature computed in the present approach is compared with Uhrig and Schulz's (US) result[23] [see Fig. 11(a)] and with Müller, Beck, and Bonner's (MBB) form[22] [see Fig. 11(b)] in the cases with and without lattice displacement, respectively. For convenience, each spectral function is normalized so as to have the integrated area to be in unity. US's calculation was based on a continuum approximation for a fermionic model with constant lattice displacement. From Fig. 11(a), we find our spectrum well resembles that of US in the line shape. The difference in the frequency range should be attributed to the different magnitude of lattice distortions, i.e., $\delta(\text{ours})/\delta(\text{US})\simeq 10$. In fact, our spectrum can move toward the lower frequency side, recovering US's result even in the frequency range, by increasing the elastic constant c and thus by decreasing $\delta(\text{ours})$ [see Figs. 8(a)–8(c)]. On the other hand, from Fig. 11(b), we find the ratios of the upper and lower frequency edges are the same in both of our and MBB's cases, i.e., $\omega(\text{upper})/\omega(\text{lower})=|\text{cosec}(k/2)|$. Some different behaviors, however, are found. One is the frequency region of the spectrum, as described before, i.e., $\Delta\Omega^{0}(\pi/2)=2.98$ for our case versus 2.85 for MBB's case. Another is the line shape in

the vicinity of the two band edges. In contrast to the divergent behavior at the lower edge and an abrupt cutoff at the upper edge in MBB's case, our result shows smooth band edges. To resolve this discrepancy, further intensive theoretical studies would be necessary.

We shall proceed to the case of finite temperatures below T_{SP} [see Figs. 8(b), 9(b), and 10(b) and Figs. 8(c), 9(c), and 10(c)], in which Fermi distributions become diffuse so that other two intraband scattering processes ($\alpha \rightarrow \alpha$ and $\gamma \rightarrow \gamma$) also give nonvanishing contributions. $\chi''_{zz}(k,\omega)$ here has two nonoverlapping structures: Besides the high-frequency part lying in $\Omega_M(k) \leqslant \Omega \leqslant \Omega_H(k)$, the low-frequency part extending to $\Omega = 0$ appears, which is limited by a very singular peak at the upper edge $\Omega_L(k)$ $[< \Omega_M(k)]$. While the former is responsible for the triplet magnon continuum excitations, the latter is caused by thermal fluctuations. As the temperature is raised from zero, the peak position and $\Omega_M(k)$ of the high-frequency part move to a lower-energy side, whereas $\Omega_L(k)$ moves in an opposite way. For reference, $\chi''^{(0)}_{zz}(k,\omega)$ without lattice coupling[18] is also illustrated by a dotted line at just below T_{SP} in Figs. 8(c), 9(c), and 10(c). At $T > T_{SP}$ (i.e., in the uniform phase), $\chi''_{zz}(k,\omega)$ bears only a single broad peak with a tail extending towards $\omega = 0$ [see Figs. 8(d), 9(d), and 10(d)]. In this way, rich structures of the dynamic susceptibility can be interpreted systematically in terms of various quasiparticle scattering processes proper to s-P phase.

Recently, several prominent features of spin dynamics were revealed from intensive neutron-scattering experiments, especially for the compound $CuGeO_3$.[8–13] (1) In s-P phase ($T \ll T_{SP}$) a gap of $\Delta \simeq 2.1$ meV in the magnetic excitation spectrum was observed at the zone center ($k = 0$).[8,10,12] This gap is called a ''triplet gap'' because its formation is caused by reducing a singlet dimer into a delocalized triplet. (2) A well-defined magnonlike mode is observed with a peak located at $\hbar\omega_p$ ($\simeq 16$ meV) $\geqslant \Delta$ at ZB ($k = \pi/2$). The asymmetric line shape is responsible for the magnon continuum.[12] (3) Besides the ''triplet gap,'' another gap is observed at the frequency higher than the peak position, which Aïn *et al.*[13] conjectured as ''solitonic gap.'' (4) At $T > T_{SP}$ the gapless spin-wave continuum appears,[12] though diffused, and the line shape shows a broad maximum.

The above experimental results accord qualitatively with the present theoretical issue, but the following facts should be noted: (1) The so-called ''triplet-gap'' at $k = 0$ is also seen in the dispersion curves for both $\Omega_M(k)$ and the peak position of the ''theoretical'' high-frequency structure at $T \rightarrow 0$ (see Fig. 12). Its value, which is slightly larger than the observed one at $T = 4$ K, can be improved by noting the temperature dependence of $\delta(T)$ (see Fig. 2). However, the ''solitonic gap'' by Aïn *et al.*[13] is not found in our Hartree-Fock approximation. To obtain this, more sophisticated treatment should be demanded. (2) The theoretical neutron-scattering spectrum given by Eq. (27) is also computed and compared with the observed result for $CuGeO_3$ in Fig. 13. The forbidden band between the higher- and lower-frequency parts predicted theoretically should be observed by nonpolarized neutron-scattering experiments, but has not yet been reported. However, the line shape of the high-frequency part, responsible for the triplet magnon continuum, resembles the observed asymmetric line shape in a sense that $S(k,\omega)$ abruptly rises at Ω just above $\Omega_M(k)$ and gradually decreases as $\Omega_H(k)$ is approached. (3) The unfamiliar dispersion of $\Omega_H(k)$ as in Fig. 7 has not yet been found experimentally. Arai *et al.*[12] pointed out a ''rampart'' or ridge of scattering surrounding a valley (at $k \simeq 0$) in the magnon continuum. This tendency is expected to reflect the nonvanishing width of the magnon continuum at $k = 0$ predicted above. (4) In the uniform phase ($T > T_{SP}$), $S(k,\omega)$ accords with the observed single broad hump, though a mutual discrepancy cannot be disregarded in the high-frequency region. (5) The peak at $\Omega_L(k)$ would not be actually observed because of its extremely singular nature. On the contrary, the variation of the broad peak lying just above $\Omega_M(k)$ should be captured when temperature crosses T_{SP}, although the observed peak position seems to remain unchanged. Since the present prediction is inevitable as long as the quasiparticle energy spectrum bifurcates to α and γ branches due to the lattice distortion, we hope future experiments to verify it.

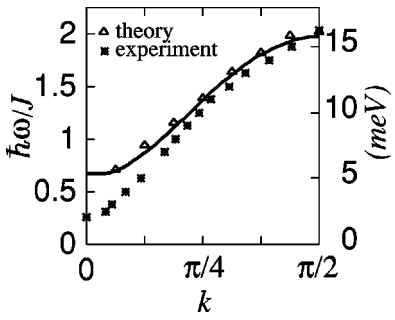

FIG. 12. Wave number dependence of Ω_M (solid lines) and theoretical peak positions (symbols $\triangle$). $J/k_B = 94$ K. Symbols (*) imply experimental peak positions (Ref. 8) at $T = 4$ K.

V. SUMMARY AND DISCUSSION

In this paper, we have theoretically investigated spin dynamics of s-P transition by incorporating the effect of temperature-dependent lattice distortion $\delta(T)$ in a self-consistent way. The expression for the generalized longitudinal susceptibility $\chi_{zz}(k,\omega)$ is derived by means of two-time Green's functions within the Hartree-Fock approximation.

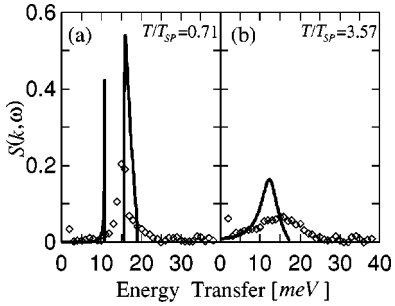

FIG. 13. Comparison between calculated spectrum (solid line) and experimental data (Ref. 12) ($\diamond$). $J/k_B = 94$ K: (a) $T/T_{SP} = 0.71$; (b) $T/T_{SP} = 3.57$. For convenience, both areas surrounded by observed spectrum and by theoretical ones are normalized to unity.

Our main results are as follows: (1) Below T_{SP}, the static susceptibility $\chi_{zz}(k,0)$ drops exponentially with decreasing temperature, going towards a small but finite value for any wave number $k\neq 0$ and to zero for $k=0$. This means the zero-point fluctuations are more or less suppressed for all nonvanishing k values and the suppression is complete for $k=0$. (2) When the temperature crosses T_{SP} from above, the first Brillouin zone becomes halved, and the quasienergy spectrum bifurcates into a pair of α and γ energy branches, for any small value of δ at $T<T_{SP}$. Consequently, four quasiparticle scattering processes predominate $\chi''_{zz}(k,\omega)$ in various ways depending on temperature. (3) At $0<T<T_{SP}$, $\chi''_{zz}(k,\omega)$ splits into the high-frequency part in $\Omega_M(k)\leqslant\Omega\leqslant\Omega_H(k)$ and the low-frequency part in $0\leqslant\Omega\leqslant\Omega_L(k)$, with $\Omega_L(k)<\Omega_M(k)$. No structure appears in the interval $\Omega_L(k)<\Omega<\Omega_M(k)$ owing to the violation of the energy conservation in the quasiparticle scattering. As T is decreased from T_{SP}, the low-frequency part tends to disappear, and the broad peak of the high-frequency part moves to a higher-energy side. At $T>T_{SP}$, $\chi''_{zz}(k,\omega)$ reduces to only a single broad maximum with a tail extending towards $\omega=0$, consistent with the earlier result.[18] (4) The high-frequency part is responsible for the triplet low-lying excitations arising from the particle-hole scattering process, while the low-frequency part is caused by thermal fluctuation due to two intraband ($\alpha\rightarrow\alpha$ and $\gamma\rightarrow\gamma$) scattering processes. (5) The dispersion of $\Omega_M(k)$ at $T\rightarrow 0$ describes the triplet low-lying excitation with a finite gap at $k=0$, and the width of the magnon continuum shows an unfamiliar increase as $k=0$ is approached.

While the above results agree qualitatively with issues of neutron scattering experiments for $CuGeO_3$, some discrepancies between them require us to reexamine the present simplified model from the following points of view: (i) It is recently argued the next-nearest-neighboring (NNN) interaction is important due to the lattice structure.[24–26] If both NN and NNN couplings are antiferromagnetic, the intrachain frustration is essential. Castilla *et al.*[24] attempted to describe the temperature dependence of the uniform susceptibility by considering both interactions. (ii) As pointed out by Hirota *et al.*,[9] $CuGeO_3$ is not an ideal 1D system, so the effect of the interchain interaction should be incorporated. (iii) We should go beyond the adiabatic treatment by including the vibrionic effect of lattice displacements. The study in these new directions will be made in due course.

ACKNOWLEDGMENTS

We are grateful to N. Maya for useful discussions. K.N. thanks A. Terai and K. Kakurai for valuable comments. This work was supported by a Grant-in-Aid for Scientific Research from the Ministry of Education, Science and Culture of Japan, No. 07640479.

APPENDIX A: FERMIONIC HAMILTONIAN WITH LATTICE DISTORTION

Applying the standard transformation,

$$S^+_{2i}=S^x_{2i}+iS^y_{2i}=b^\dagger_{2i}\exp\left[i\pi\left(\sum_{j=1}^{i-1}b^\dagger_{2j}b_{2j}+\sum_{j=1}^{i}a^\dagger_{2j-1}a_{2j-1}\right)\right],$$

$$S^+_{2i+1}=S^x_{2i+1}+iS^y_{2i+1}=a^\dagger_{2i+1}\exp\left[i\pi\left(\sum_{j=1}^{i}b^\dagger_{2j}b_{2j}+\sum_{j=1}^{i-1}a^\dagger_{2j+1}a_{2j+1}\right)\right],$$

$$S^z_{2i+1}=a^\dagger_{2i+1}a_{2i+1}-\frac{1}{2},$$

$$S^z_{2i}=b^\dagger_{2i}b_{2i}-\frac{1}{2}, \tag{A1}$$

the Hamiltonian with lattice distortion in Eq. (1) reduces to[17]

$$\mathcal{H}=\sum_\lambda\left[J(\lambda)a^\dagger_\lambda b_\lambda+J^*(\lambda)b^\dagger_\lambda a_\lambda-\frac{1}{2}(J_1+J_2)(a^\dagger_\lambda a_\lambda+b^\dagger_\lambda b_\lambda)\right]+\frac{2}{N}\sum_{\lambda_1+\lambda_2=\lambda_3+\lambda_4}J(\lambda_4-\lambda_1)b^\dagger_{\lambda_1}a^\dagger_{\lambda_2}a_{\lambda_3}b_{\lambda_4}+NC\epsilon^2, \tag{A2}$$

where $J(\lambda)$ is defined in Eq. (4). In Eq. (A2), Fourier transformation of a_{2i-1}, b_{2i},

$$a_{2i-1}=\frac{1}{\sqrt{N}}\sum_\lambda e^{-i\lambda r_{2i-1}}a_\lambda,$$

$$b_{2i}=\frac{1}{\sqrt{N}}\sum_\lambda e^{-i\lambda r_{2i}}b_\lambda, \tag{A3}$$

and its Hermitian conjugate are used. The wave number λ is determined by the periodic boundary condition as $\lambda=\pi p/N$ with $-N/2\leqslant p\leqslant N/2-1$.

By use of new fermions α_λ, γ_λ via the canonical transformation

$$a_\lambda = \left(\frac{1}{\sqrt{2}}\right)(\alpha_\lambda + \gamma_\lambda)\exp(i\phi_\lambda/2),$$

$$b_\lambda = \left(\frac{1}{\sqrt{2}}\right)(\alpha_\lambda - \gamma_\lambda)\exp(-i\phi_\lambda/2), \tag{A4}$$

with a phase factor in Eq. (4), $\mathcal{H}$ in Eq. (A2) reduces to the fermionic Hamiltonian in Eq. (2).

APPENDIX B: DERIVATION OF EQ. (21) AND RELATED COEFFICIENTS

The decoupled equations of motion for Green's functions multiplied by phase factors are given by

$$\begin{aligned}(\hbar\omega - \varepsilon^\alpha_{\lambda-k} + \varepsilon^\alpha_\lambda)\sum_\mu \exp\left[\frac{i}{2}(\phi_{\mu+k} - \phi_\mu)\right]\langle\langle \alpha^\dagger_\lambda \alpha_{\lambda-k} | \alpha^\dagger_\mu \alpha_{\mu+k}\rangle\rangle_\omega \\ = \exp\left[\frac{i}{2}(\phi_\lambda - \phi_{\lambda-k})\right](n^\alpha_\lambda - n^\alpha_{\lambda-k}) + (n^\alpha_\lambda - n^\alpha_{\lambda-k})\frac{1}{N}\sum_\mu\sum_\nu \frac{1}{2}(W_1 - W_2) \\ \times \exp\left[\frac{i}{2}(\phi_{\mu+k} - \phi_\mu)\right]\langle\langle \alpha^\dagger_\nu \alpha_{\nu-k} | \alpha^\dagger_\mu \alpha_{\mu+k}\rangle\rangle_\omega,\end{aligned} \tag{B1}$$

where

$$W_1 = J_1\cos\left[-k(1-\delta) + \frac{1}{2}(\phi_{\lambda-k} - \phi_\nu + \phi_{\nu-k} - \phi_\lambda)\right] + J_2\cos\left[k(1+\delta) + \frac{1}{2}(\phi_{\lambda-k} - \phi_\nu + \phi_{\nu-k} - \phi_\lambda)\right],$$

$$W_2 = J_1\cos\left[-(\lambda-\nu)(1-\delta) + \frac{1}{2}(\phi_\nu - \phi_{\lambda-k} + \phi_{\nu-k} - \phi_\lambda)\right] + J_2\cos\left[(\lambda-\nu)(1+\delta) + \frac{1}{2}(\phi_{\lambda-k} - \phi_\nu + \phi_{\nu-k} - \phi_\lambda)\right]. \tag{B2}$$

A set of equations in Eqs. (B1) and (B2) can be rewritten more elegantly by introducing the variables X and Y in Eq. (19), where Q and R are defined as

$$Q_1(k;\lambda) = \cos\left[\frac{1}{2}(\phi_{\lambda-k} - \phi_\lambda)\right],$$

$$Q_3(k;\lambda) = \cos\left[\lambda(1-\delta) + \frac{1}{2}(\phi_{\lambda-k} + \phi_\lambda)\right],$$

$$Q_5(k;\lambda) = \cos\left[-\lambda(1+\delta) + \frac{1}{2}(\phi_{\lambda-k} + \phi_\lambda)\right],$$

and

$$R_1(k;\lambda) = J_1\cos\left[-k(1-\delta) + \frac{1}{2}(\phi_{\lambda-k} - \phi_\lambda)\right] + J_2\cos\left[k(1+\delta) + \frac{1}{2}(\phi_{\lambda-k} - \phi_\lambda)\right],$$

$$R_3(k;\lambda) = J_1\cos\left[\lambda(1-\delta) + \frac{1}{2}(\phi_{\lambda-k} + \phi_\lambda)\right],$$

$$R_5(k;\lambda) = J_2\cos\left[-\lambda(1+\delta) + \frac{1}{2}(\phi_{\lambda-k} + \phi_\lambda)\right]. \tag{B3}$$

Q_2, Q_4, Q_6, R_2, R_4, R_6 are given by replacing ''cos'' by ''sin'' in the above definitions for Q_1, Q_3, Q_5, R_1, R_3, R_5, respectively. We easily have the algebraic equations in Eq. (21), whose coefficients are given by

$$A^{uv}=\begin{pmatrix} 1-\Gamma^{uv}_{1,1} & \Gamma^{uv}_{1,2} & \Gamma^{uv}_{1,3} & \Gamma^{uv}_{1,4} & \Gamma^{uv}_{1,5} & \Gamma^{uv}_{1,6} \\ -\Gamma^{uv}_{2,1} & 1+\Gamma^{uv}_{2,2} & \Gamma^{uv}_{2,3} & \Gamma^{uv}_{2,4} & \Gamma^{uv}_{2,5} & \Gamma^{uv}_{2,6} \\ -\Gamma^{uv}_{3,1} & \Gamma^{uv}_{3,2} & 1+\Gamma^{uv}_{3,3} & \Gamma^{uv}_{3,4} & \Gamma^{uv}_{3,5} & \Gamma^{uv}_{3,6} \\ -\Gamma^{uv}_{4,1} & \Gamma^{uv}_{4,2} & \Gamma^{uv}_{4,3} & 1+\Gamma^{uv}_{4,4} & \Gamma^{uv}_{4,5} & \Gamma^{uv}_{4,6} \\ -\Gamma^{uv}_{5,1} & \Gamma^{uv}_{5,2} & \Gamma^{uv}_{5,3} & \Gamma^{uv}_{5,4} & 1+\Gamma^{uv}_{5,5} & \Gamma^{uv}_{5,6} \\ -\Gamma^{uv}_{6,1} & \Gamma^{uv}_{6,2} & \Gamma^{uv}_{6,3} & \Gamma^{uv}_{6,4} & \Gamma^{uv}_{6,5} & 1+\Gamma^{uv}_{6,6} \end{pmatrix} \tag{B4a}$$

$$(uv=\alpha\alpha,\gamma\gamma),$$

$$A^{uv}=\begin{pmatrix} 1+\Gamma^{uv}_{1,1} & -\Gamma^{uv}_{1,2} & \Gamma^{uv}_{1,3} & \Gamma^{uv}_{1,4} & \Gamma^{uv}_{1,5} & \Gamma^{uv}_{1,6} \\ \Gamma^{uv}_{2,1} & 1-\Gamma^{uv}_{2,2} & \Gamma^{uv}_{2,3} & \Gamma^{uv}_{2,4} & \Gamma^{uv}_{2,5} & \Gamma^{uv}_{2,6} \\ \Gamma^{uv}_{3,1} & -\Gamma^{uv}_{3,2} & 1+\Gamma^{uv}_{3,3} & \Gamma^{uv}_{3,4} & \Gamma^{uv}_{3,5} & \Gamma^{uv}_{3,6} \\ \Gamma^{uv}_{4,1} & -\Gamma^{uv}_{4,2} & \Gamma^{uv}_{4,3} & 1+\Gamma^{uv}_{4,4} & \Gamma^{uv}_{4,5} & \Gamma^{uv}_{4,6} \\ \Gamma^{uv}_{5,1} & -\Gamma^{uv}_{5,2} & \Gamma^{uv}_{5,3} & \Gamma^{uv}_{5,4} & 1+\Gamma^{uv}_{5,5} & \Gamma^{uv}_{5,6} \\ \Gamma^{uv}_{6,1} & -\Gamma^{uv}_{6,2} & \Gamma^{uv}_{6,3} & \Gamma^{uv}_{6,4} & \Gamma^{uv}_{6,5} & 1+\Gamma^{uv}_{6,6} \end{pmatrix} \tag{B4b}$$

$$(uv=\alpha\gamma,\gamma\alpha)$$

with

$$\Gamma^{uv}_{m,n}\equiv\frac{1}{N}\sum_{\lambda}\frac{1}{2}R_m(k;\lambda)Q_n(k;\lambda)\mathcal{G}^{uv}_k(\lambda). \tag{B4c}$$

On the rhs of Eq. (21), C and S are defined by

$$C^{uv}_n\equiv\frac{1}{N}\sum_{\lambda}\cos\left[\frac{1}{2}(\phi_\lambda-\phi_{\lambda-k})\right]\mathcal{G}^{uv}_k(\lambda)Q_n(k;\lambda),$$

$$S^{uv}_n\equiv\frac{1}{N}\sum_{\lambda}\sin\left[\frac{1}{2}(\phi_\lambda-\phi_{\lambda-k})\right]\mathcal{G}^{uv}_k(\lambda)Q_n(k;\lambda). \tag{B5}$$

The Green's function $\mathcal{G}^{vu}_k(\lambda)$ in Eqs. (B4) and (B5) is given in Eq. (22).

[1] R. E. Peierls, *Quantum Theory of Solids* (Clarendon Press, Oxford, 1955).

[2] H. M. McConnell and R. Lynden-Bell, J. Chem. Phys. **36**, 2393 (1962); D. D. Thomas, H. Keller, and H. M. McConnell, *ibid.* **39**, 2321 (1963); D. B. Chesnut, *ibid.* **45**, 4677 (1966).

[3] J. W. Bray, H. R. Hart, Jr., L. V. Interrante, I. S. Jacobs, J. S. Kasper, G. D. Watkins, S. H. Wee, and J. C. Bonner, Phys. Rev. Lett. **35**, 744 (1975); I. S. Jacobs, J. W. Bray, H. R. Hart, Jr., L. V. Interrante, J. S. Kasper, G. D. Watkins, D. E. Prober, and J. C. Bonner, Phys. Rev. B **14**, 3036 (1976).

[4] J. W. Bray, L. V. Interrante, I. S. Jacobs, and J. C. Bonner, in *Extended Linear Chain Compounds*, edited by J. S. Miller (Plenum, New York, 1983), Vol. 3, p. 353, and references cited therein.

[5] J. H. H. Perk and H. W. Capel, Physica A **100**, 1 (1980); J. C. Bonner and H. W. J. Blöte, Phys. Rev. B **25**, 6959 (1982); J. H. Taylor and G. Müller, Physica A **130**, 1 (1985).

[6] M. Hase, I. Terasaki, and K. Uchinokura, Phys. Rev. Lett. **70**, 3651 (1993).

[7] Q. J. Harris, Q. Feng, R. J. Birgeneau, K. Hirota, K. Kakurai, J. E. Lorenzo, G. Shirane, M. Hase, K. Uchinokura, H. Kojima, I. Tanaka, and Y. Shibuya, Phys. Rev. B **50**, 12 606 (1994).

[8] M. Nishi, O. Fujita, and J. Akimitsu, Phys. Rev. B **50**, 6508 (1994).

[9] K. Hirota, D. E. Cox, J. E. Lorenzo, G. Shirane, J. M. Tranquada, M. Hase, K. Uchinokura, H. Kojima, Y. Shibuya, and I. Tanaka, Phys. Rev. Lett. **73**, 736 (1994).

[10] L. P. Regnault, M. Aïn, B. Hennion, G. Dhalenne, and A. Revcolevschi, Phys. Rev. B **53**, 5579 (1996).

[11] M. C. Martin, G. Shirane, Y. Fujii, M. Nishi, O. Fujita, J. Akimitsu, M. Hase, and K. Uchinokura, Phys. Rev. B **53**, R14 713 (1996).

[12] M. Arai, M. Fujita, M. Motokawa, J. Akimitsu, and S. M. Bennington, Phys. Rev. Lett. **77**, 3649 (1996).

[13] M. Aïn, J. E. Lorenzo, L. P. Regnault, G. Dhalenne, A. Revcolevschi, B. Hennion, and Th. Jolicoeur, Phys. Rev. Lett. **78**, 1560 (1997).

[14] K. Kawasaki, N. Maya, A. Kouzuki, and K. Nakamura, J. Phys. Soc. Jpn. **66**, 839 (1997).

[15] A. Luther and I. Peschel, Phys. Rev. B **9**, 2911 (1974); **12**, 3908 (1975); S. Coleman, Phys. Rev. D **11**, 2088 (1975); M. C. Cross and D. S. Fisher, Phys. Rev. B **19**, 402 (1979).

[16] D. N. Zubarev, Usp. Fiz. Nauk **71**, 71 (1960) [Sov. Phys. Usp. **3**, 320 (1960)].
[17] L. N. Bulaevskii, Zh. Éksp. Theor. Fiz. **44**, 1008 (1963) [Sov. Phys. JETP **17**, 684 (1963)]; G. Beni, J. Chem. Phys. **58**, 3200 (1973).
[18] T. Todani and K. Kawasaki, Prog. Theor. Phys. **50**, 1216 (1973).
[19] J. C. Bonner and M. E. Fisher, Phys. Rev. **135**, A640 (1964).
[20] W. Marshall and S. W. Lovesey, *Theory of Thermal Neutron Scattering* (Clarendon Press, Oxford, 1971).
[21] J. des Cloizeaux and J. J. Pearson, Phys. Rev. **128**, 2131 (1962); D. C. Mattis, *The Theory of Magnetism I* (Springer, Berlin, 1981).
[22] G. Müller, H. Beck, and J. C. Bonner, Phys. Rev. Lett. **43**, 75 (1979).
[23] Götz S. Uhrig and H. J. Schulz, Phys. Rev. B **54**, R9624 (1996).
[24] G. Castilla, S. Chakravarty, and V. J. Emery, Phys. Rev. Lett. **75**, 1823 (1995).
[25] J. Riera and A. Dobry, Phys. Rev. B **51**, 16 098 (1995).
[26] K. Fabricius, A. Klümper, U. Löw, B. Büchner, T. Lorenz, G. Dhalenne, and A. Revcolevschi, Phys. Rev. B **57**, 1102 (1998).